Approaching the neutron-rich heavy and superheavy nuclei by multinucleon transfer reactions with radioactive isotopes

Peng-Hui Chen,[1,2] Fei Niu,[3] Wei Zuo,[1,2] and Zhao-Qing Feng[3,*]

[1]*Institute of Modern Physics, Chinese Academy of Sciences, Lanzhou 730000, China*

[2]*School of Nuclear Science and Technology, University of Chinese Academy of Sciences, Beijing 100190, China*

[3]*School of Physics and Optoelectronics, South China University of Technology, Guangzhou 510640, China*

(Received 29 September 2019; revised manuscript received 18 January 2020; accepted 11 February 2020; published 27 February 2020)

The dynamical mechanism of multinucleon transfer reactions was investigated within the dinuclear system model, in which the sequential nucleon transfer is described by solving a set of microscopically derived master equations. Production cross sections, total kinetic energy spectra, and angular distribution of formed fragments in the reactions of ^{124,132}Sn + ^{238}U/^{248}Cm near Coulomb barrier energies are thoroughly analyzed. It is found that the total kinetic energies of primary fragments are dissipated from the relative motion energy and rotational energy of the two colliding nuclei. The fragments are formed in the forward angle domain. The energy dependence of the angular spectra is different between projectilelike and targetlike fragments. Isospin equilibrium is governed under the potential energy surface. The production cross sections of neutron-rich isotopes are enhanced around the shell closure.

DOI: 10.1103/PhysRevC.101.024610

I. INTRODUCTION

The synthesis of superheavy nuclei (SHN) has obtained much progress up to element $Z = 118$ (Oganesson) in cold fusion reactions [1] and by ^{48}Ca-induced reactions [2] in terrestrial laboratories. However, the observed isotopes are positioned away from the island of stability because of the deficiency of neutrons. For eliminating the problem, the fusion-evaporation reactions induced by radioactive nuclides or the multinucleon transfer (MNT) reactions might be potentionally a way to approach the island. Meanwhile, it remains a topical subject in various laboratories and appropriate separation and detection techniques are in development [3]. Because of the broader excitation functions of MNT products, it has the advantage that a wide region of isotopes can be populated in one experiment while complete fusion reactions are selective for only a few isotopes at a given beam energy and experimental setting. On the other hand, the properties of neutron-rich heavy isotopes are crucial in understanding the origin of heavy elements from iron to uranium in the r process of astrophysics. Traditionally, the neutron-rich isotopes are produced via the different mechanism by the fission of transactinide nuclides, projectile fragmentation, and complete fusion reactions for the light and medium mass regions. However, extending to the heavy mass domain and even to the island of superheavy stability, it is limited by the neutron abundance of projectile-target systems in the fusion-evaporation reactions. The MNT might be a possible way to produce the neutron-rich heavy isotopes in the nuclear chart [4–6].

Following the motivation for producing heavy new isotopes and approaching the neutron-rich SHN, several models have been developed for describing the transfer reactions, i.e., the dynamical model based on multidimensional Langevin equations [7], the time-dependent Hartree-Fock (TDHF) approach [8–11], the GRAZING model [12,13], the improved quantum molecular dynamics (ImQMD) model [14], and the dinuclear system (DNS) model [15,16], etc. Some interesting issues have been stressed, e.g., the production cross sections of new isotopes, total kinetic energy spectra of transfer fragments, and the structure effect on the fragment formation. There are still some open problems for the transfer reactions, i.e., the mechanism of preequilibrium cluster emission, the stiffness of the nuclear surface during the nucleon transfer process, the mass limit of new isotopes with stable heavy target nuclides, etc. The extremely neutron-rich beams are favorable for creating neutron-rich heavy or superheavy nuclei owing to the isospin equilibrium [17]. More discussions on the advantage of radioactive isotopes in MNT reactions may be referred to in [18–20].

The transfer reactions and deep inelastic heavy-ion collisions were extensively investigated in experiments since the 1970s, in which the new neutron-rich isotopes of light nuclei and proton-rich actinide nuclei were observed [21–27]. The reaction mechanism and fragment formation were investigated thoroughly, i.e., the energy and angular momentum dissipation, two-body kinematics, shell effect, fission of actinide nuclei, etc. Recently, more measurements have been performed at different laboratories for creating the neutron-rich heavy nuclei, e.g., the reactions of ^{136}Xe + ^{208}Pb [5,28], ^{136}Xe + ^{198}Pt [6], ^{156,160}Gd + ^{186}W [29], and ^{238}U + ^{232}Th [30]. It was shown that the MNT reactions are feasible for

*fengzhq@scut.edu.cn

producing new isotopes. Synthesis of neutron-rich SHN beyond Z=105 via the MNT reactions have been arranged at the High Intensity Heavy-Ion Facility (HIAF) in the near future [31].

In this work, the MNT reactions with the combinations of ^{124,132}Sn + ^{238}U/ ^{248}Cm are calculated with the DNS model. The article is organized as follows: In Sec. II we give a brief description of the DNS model. Calculated results and discussions are presented in Sec. III. Summary is concluded in Sec. IV.

II. MODEL DESCRIPTION

The DNS concept was proposed by Volkov for describing the deep inelastic heavy-ion collisions [32], in which a few-nucleon transfer was treated. Application of the approach to superheavy nucleus formation via massive fusion reactions in competition with the quasifission process was used for the first time by Adamian *et al.* [33,34]. The modifications of the relative motion energy and angular momentum of two colliding nuclei coupling to nucleon transfer within the DNS concept were performed by the Lanzhou group [35–37]. The production cross sections of SHN, quasifission, and fusion-fission dynamics have been extensively investigated within the DNS model [38,39]. The dynamical evolution of colliding system sequentially proceeds the capture process by overcoming the Coulomb barrier to form the DNS, relaxation process of the relative motion energy, angular momentum, mass and charge asymmetry, etc., within the potential energy surface and the de-excitation of primary fragments. The cross sections of the primary and secondary fragments produced in the MNT reactions are evaluated by

$$\sigma_{pr}(Z_1, N_1, E_{\mathrm{c.m.}}) = \frac{\pi\hbar^2}{2\mu E_{\mathrm{c.m.}}} \sum_{J=0}^{J_{\max}} (2J+1) \times \int f(B) T(E_{\mathrm{c.m.}}, J, B) \times P(Z_1, N_1, E_1, J_1, B) dB, \quad (1)$$

and

$$\sigma_{\mathrm{sur}}(Z_1, N_1, E_{\mathrm{c.m.}}) = \frac{\pi\hbar^2}{2\mu E_{\mathrm{c.m.}}} \sum_{J=0}^{J_{\max}} (2J+1) \times \int f(B) T(E_{\mathrm{c.m.}}, J, B) \times \sum_{s} P(Z_1', N_1', E_1', J_1', B) \times W_{\mathrm{sur}}(Z_1', N_1', E_1', J_1', s) dB, \quad (2)$$

respectively. The μ is the reduced mass of relative motion in the colliding system. The transmission probability $T(E_{\mathrm{c.m.}}, J)$ is taken as zero and unity corresponding to the incident energy $E_{\mathrm{c.m.}}$ in the center-of-mass frame below and above the summation value of attempting barrier B and rotational energy at the relative angular momentum J. The E_1 and J_1 are the excitation energy and the angular momentum for the fragment (Z_1, N_1). The maximal angular momentum $J_{\max}$ is taken to be the grazing collision of two nuclei. The survival probability W_{sur} of each fragment is evaluated with a statistical approach based on the Weisskopf evaporation theory [40], in which the excited primary fragments are cooled in evaporation channels $s(Z_s, N_s)$ by γ rays, light particles (neutrons, protons, α, etc.) in competition with the binary fission via $Z_1 = Z_1' - Z_s$ and $N_1 = N_1' - N_s$. The structure effects are embodied via the potential energy surface in the formation of the primary fragments, i.e., shell correction, odd-even effect, Q value, etc. The transferred cross section is smoothed with the barrier distribution and the function is taken as the Gaussian form of $f(B) = \frac{1}{N} \exp[-((B - B_m)/\Delta)^2]$ with the normalization constant satisfying the unity relation $\int f(B) dB = 1$. The quantities B_m and Δ are evaluated by $B_m = (B_C + B_S)/2$ and $\Delta = (B_C - B_S)/2$, respectively. The B_C and B_S are the Coulomb barrier at waist-to-waist orientation and the minimum barrier with varying the quadrupole deformation parameters of colliding partners. It should be noticed that there are no potential pockets for the heavy systems. The existence of the pocket in the entrance channel is crucial for the compound nucleus formation in fusion reactions [41]. In this work, the barrier is taken as the potential value at the touching configuration and the nucleus-nucleus potential is calculated with the same approach in fusion reactions [37]. The lifetime of the DNS is strongly reduced in the MNT reactions in comparison to the fusion-evaporation reactions, i.e., the relaxation time being 40×10^{-22}s for the system ^{124}Sn + ^{238}U and 200×10^{-22}s for the reaction ^{48}Ca + ^{208}Pb.

The distribution probability is obtained by solving a set of master equations numerically in the potential energy surface of the DNS. The time evolution of the distribution probability $P(Z_1, N_1, E_1, J_1, B, t)$ for fragment 1 with proton number Z_1, neutron number N_1, excitation energy E_1, angular momentum J_1, and barrier B is described by the following master equations:

$$\frac{dP(Z_1, N_1, E_1, J_1, B, t)}{dt} = \sum_{Z_1'} W_{Z_1,N_1;Z_1',N_1}(t)[d_{Z_1,N_1} P(Z_1', N_1, E_1', J_1, B, t) - d_{Z_1',N_1} P(Z_1, N_1, E_1, J_1, B, t)] + \sum_{N_1'} W_{Z_1,N_1;Z_1,N_1'}(t)[d_{Z_1,N_1} P(Z_1, N_1', E_1', J_1, B, t) - d_{Z_1,N_1'} P(Z_1, N_1, E_1, J_1, B, t)]. \quad (3)$$

Here the $W_{Z_1,N_1;Z_1',N_1}(W_{Z_1,N_1;Z_1,N_1'})$ is the mean transition probability from the channel (Z_1, N_1, E_1) to (Z_1', N_1, E_1'), [or (Z_1, N_1, E_1) to (Z_1, N_1', E_1')], and d_{Z_1,Z_1} denotes the microscopic dimension corresponding to the macroscopic state (Z_1, N_1, E_1).The sum is taken over all possible proton and neutron numbers that fragment Z_1', N_1' may take, but only one nucleon transfer is considered in the model with the relations $Z_1' = Z_1 \pm 1$ and $N_1' = N_1 \pm 1$. It is noticed that the decay of DNS is not taken into account because of the vanishing quasifission barrier, which was included in the fusion-evaporation reactions [38,39]. Actually, the decay of the DNS was effectively considered with shortening the interaction time.

The motion of nucleons in the interacting potential is governed by the single-particle Hamiltonian. The excited DNS opens a valence space in which the valence nucleons have a symmetrical distribution around the Fermi surface. Only the particles at the states within the valence space are actively for nucleon transfer. The transition probability is related to the local excitation energy and nucleon transfer, which is microscopically derived from the interaction potential in valence space as

$$W_{Z_1,N_1;Z_1',N_1} = \frac{\tau_{\rm mem}(Z_1,N_1,E_1;Z_1',N_1,E_1')}{d_{Z_1,N_1}d_{Z_1',N_1}\hbar^2} \times \sum_{ii'}|\langle Z_1',N_1,E_1',i'|V|Z_1,N_1,E_1,i\rangle|^2. \quad (4)$$

The transition coefficients determine the distribution width of the isotopic yields in the MNT reactions. The memory time is calculated by

$$\tau_{\rm mem}(Z_1,N_1,E_1;Z_1',N_1,E_1') = \left[\frac{2\pi\hbar^2}{\sum_{KK'}\langle V_{KK}V_{KK'}^*\rangle}\right]^{1/2}, \quad (5)$$

$$\langle V_{KK}V_{KK'}^*\rangle = \tfrac{1}{4}U_{KK'}^2 g_K g_K' \Delta_{KK'}\Delta\varepsilon_K\Delta\varepsilon_K', \times\left[\Delta_{KK'}^2 + \tfrac{1}{6}((\Delta\varepsilon_K)^2 + (\Delta\varepsilon_K')^2)\right]^{-1/2}. \quad (6)$$

The interaction matrix element is given by

$$\sum_{ii'}|V_{ii'}|^2 = [\omega_{11}(Z_1,N_1,E_1,E_1') + \omega_{22}(Z_1,N_1,E_1,E_1')]\delta_{Z_1,N_1,E_1;Z_1,N_1,E_1'} + \omega_{12}(Z_1,N_1,E_1,E_1')\delta_{Z_1',N_1,E_1;Z_1-1,N_1,E_1'} + \omega_{21}(Z_1,N_1,E_1,E_1')\delta_{Z_1',N_1,E_1;Z_1+1,N_1,E_1'}, \quad (7)$$

with the relation of

$$\omega_{KK'}(Z_1,N_1,E_1,E_1') = d_{Z_1,N_1}\langle V_{KK'}V_{KK'}^*\rangle. \quad (8)$$

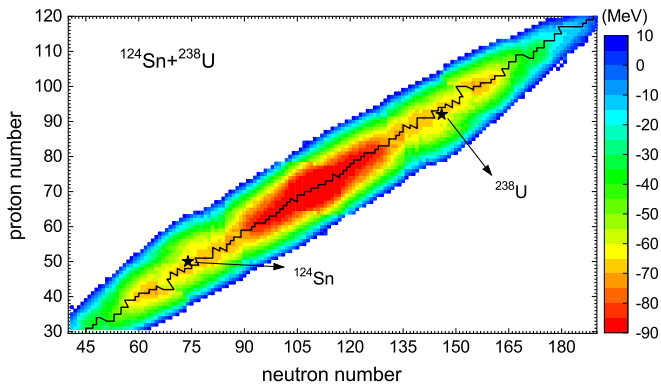

FIG. 1. Potential energy surface in the reaction of ^{124}Sn + ^{238}U and the black line corresponding to the minimum value of each isotopic chain.

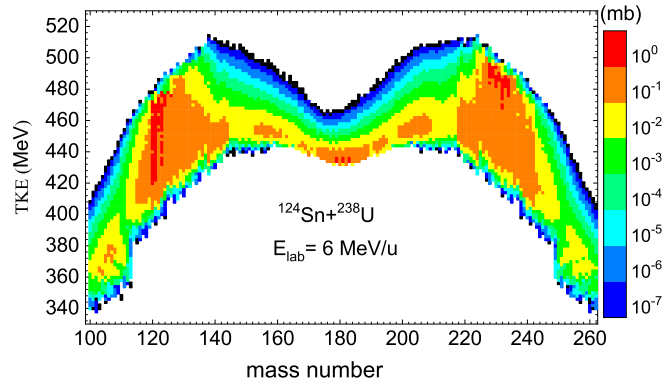

FIG. 2. Mass distribution of total kinetic energy of the primary binary fragments in the reaction of ^{124}Sn + ^{238}U at the incident energy $E_{\rm lab} = 6$ MeV/nucleon.

A similar approach is used for the neutron transition coefficient.

The averages on these quantities are performed in the valence space as follows [42]:

$$\Delta\varepsilon_K = \sqrt{\frac{4\varepsilon_K^*}{g_K}}, \quad \varepsilon_K^* = \varepsilon^*\frac{A_K}{A}, \quad g_K = A_K/12, \quad (9)$$

where the ε^* is the local excitation energy of the DNS. The microscopic dimension for the fragment (Z_K, N_K) is evaluated by the valence states $N_K = g_K\Delta\varepsilon_K$ and the valence nucleons $m_K = N_K/2$ $(K = 1, 2)$ as

$$d(m_1,m_2) = \binom{N_1}{m_1}\binom{N_2}{m_2}. \quad (10)$$

In the relaxation process of the relative motion, the DNS will be excited by the dissipation of the relative kinetic energy. The local excitation energy is determined by the dissipation energy from the relative motion and the potential energy

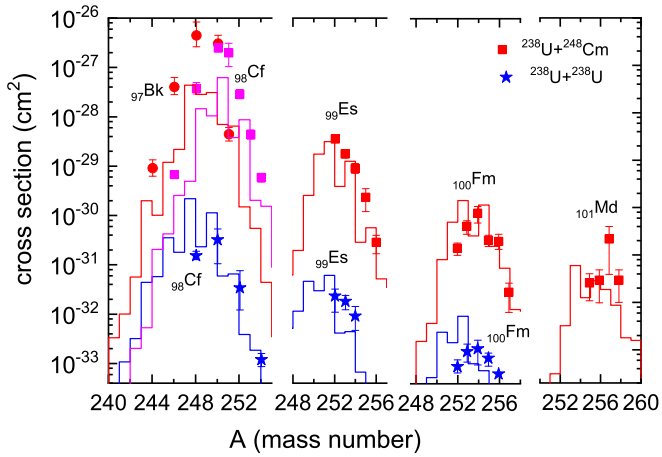

FIG. 3. Production cross sections of transcurium isotopes in the ^{238}U + ^{238}U reaction and ^{238}U + ^{248}Cm reaction at $E_{\rm lab} = 7.0$ MeV/nucleon and compared with the available experimental data at GSI with error bars [46].

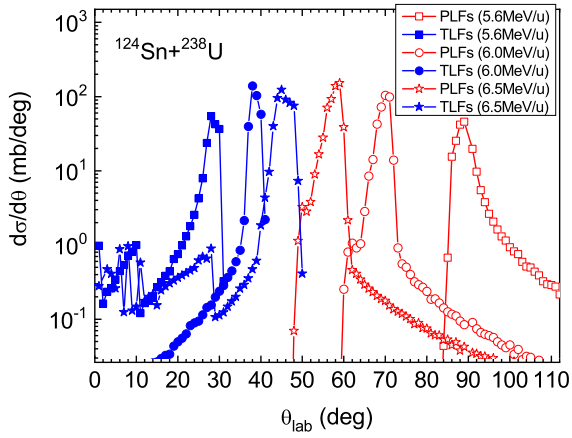

FIG. 4. Angular distributions of the Sn-like (blue lines) and the U-like products (red lines) in the laboratory frame at different energies.

surface of the DNS as

$$\varepsilon^*(t) = E^{\rm diss}(t) - (U(\{\alpha\}) - U(\{\alpha_{\rm EN}\})). \tag{11}$$

The entrance channel quantities $\{\alpha_{\rm EN}\}$ include the proton and neutron numbers, quadrupole deformation parameters, and orientation angles being Z_P, N_P, Z_T, N_T, R, β_P, β_T, θ_P, θ_T for projectile and target nuclei with the symbols of P and T, respectively. The excitation energy E_1 for fragment (Z_1,N_1) is evaluated by $E_1 = \varepsilon^*(t = \tau_{\rm int})A_1/A$. The interaction time $\tau_{\rm int}$ is obtained from the deflection function method [43]. The energy dissipated into the DNS is expressed as

$$E^{\rm diss}(t) = E_{\rm c.m.} - B - \frac{\langle J(t)\rangle[\langle J(t)\rangle + 1]\hbar^2}{2\zeta} - \langle E_{\rm rad}(J,t)\rangle. \tag{12}$$

Here $E_{\rm c.m.}$ and B are the center-of-mass energy and Coulomb barrier, respectively. The radial energy is evaluated from

$$\langle E_{\rm rad}(J,t)\rangle = E_{\rm rad}(J,0)\exp(-t/\tau_r). \tag{13}$$

The relaxation time of the radial motion $\tau_r = 5 \times 10^{-22}$ s and the radial energy at the initial state $E_{\rm rad}(J,0) = E_{\rm c.m.} - B - J_i(J_i+1)\hbar^2/(2\zeta_{\rm rel})$. The dissipation of the relative angular momentum is described by

$$\langle J(t)\rangle = J_{st} + (J_i - J_{st})\exp(-t/\tau_J). \tag{14}$$

The angular momentum at the sticking limit $J_{st} = J_i\zeta_{\rm rel}/\zeta_{\rm tot}$ and the relaxation time $\tau_J = 15 \times 10^{-22}$ s. The $\zeta_{\rm rel}$ and $\zeta_{\rm tot}$ are the relative and total moments of inertia of the DNS, respectively, in which the quadrupole deformations are implemented [44]. The initial angular momentum is set to be $J_i = J$ in the following work. In the relaxation process of the relative motion, the DNS will be excited by the dissipation of the relative kinetic energy.

The local excitation energy is determined by the excitation energy of the composite system and the potential energy surface (PES) of the DNS. The PES is evaluated by

$$U(\{\alpha\}) = B(Z_1,N_1) + B(Z_2,N_2) - B(Z,N) + V(\{\alpha\}), \tag{15}$$

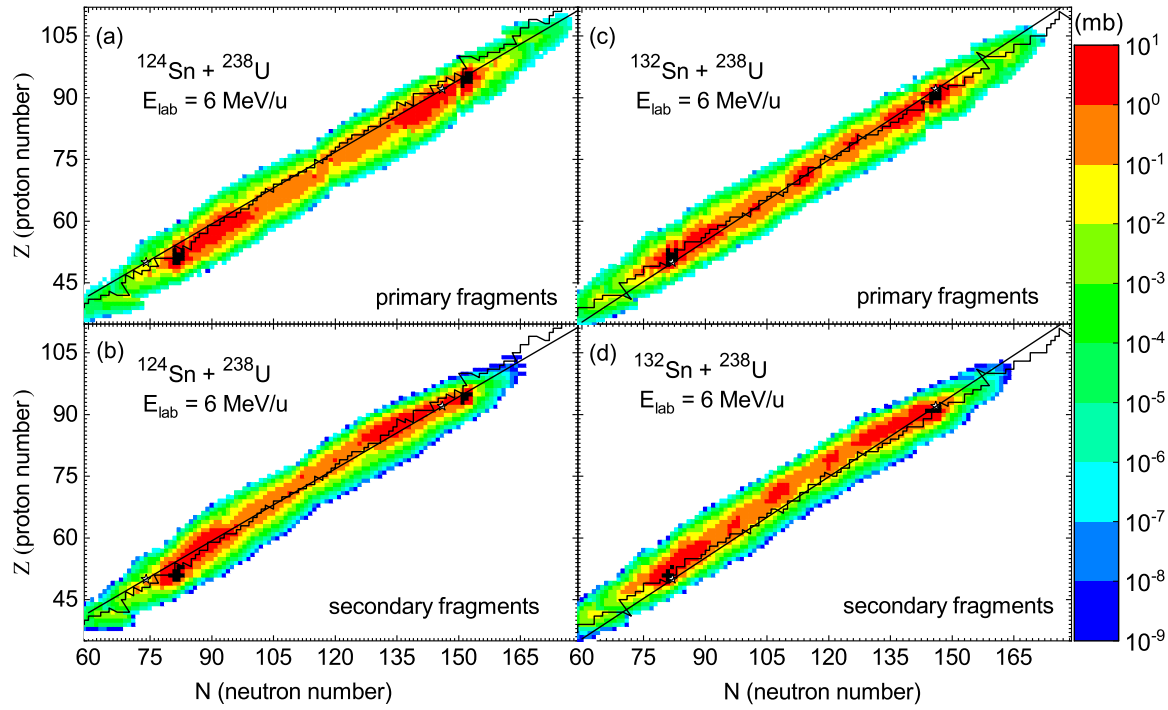

FIG. 5. Contour plot of production cross sections as functions of neutron and proton numbers of primary fragments and secondary fragments in collisions of ^{124}Sn/^{132}Sn + ^{238}U at the incident energy of 6 MeV/nucleon. The zigzag and straight lines correspond to the minimal values of PES and to the neutron-proton line of the target-projectile combination.

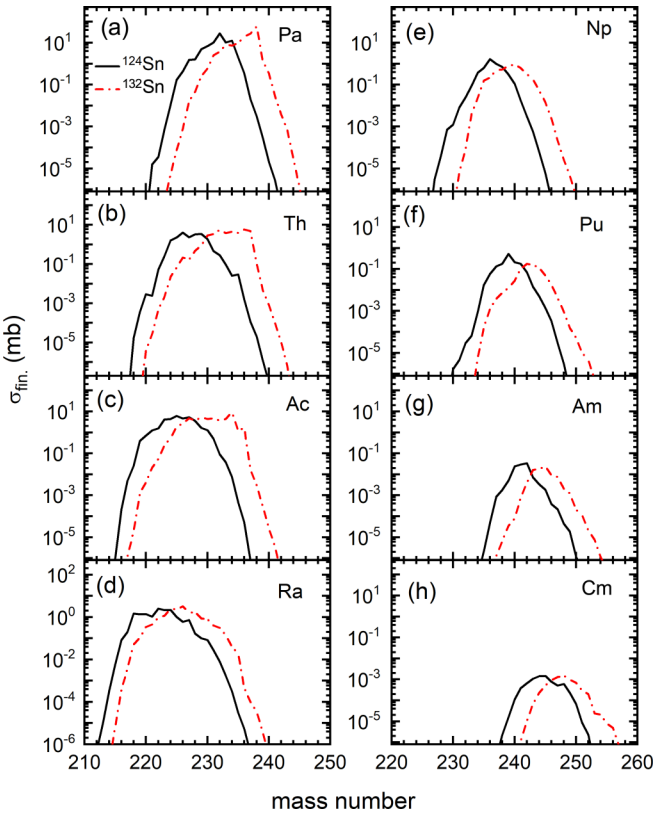

FIG. 6. Production cross sections of different channels in collisions of ^{124}Sn and ^{132}Sn on ^{238}U at the incident energy 6 MeV/nucleon.

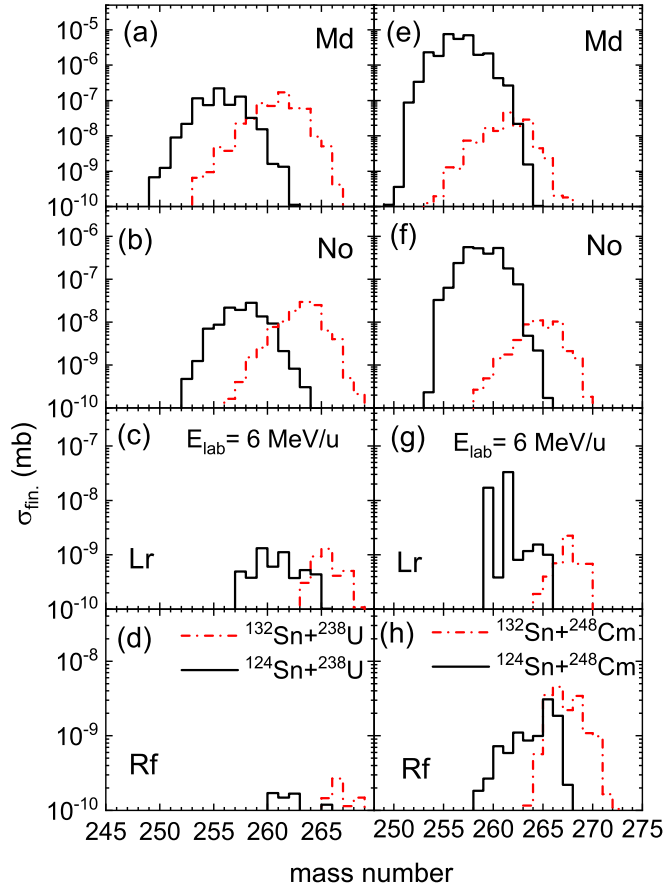

FIG. 7. Comparison of isotopic cross sections for producing elements of $Z = 101$–104 with the ^{238}U- (left panels) and ^{248}Cm-based reactions (right panels) at the incident energy of 6 MeV/nucleon.

which satisfies the relation of $Z_1 + Z_2 = Z$ and $N_1 + N_2 = N$ with Z and N being the proton and neutron numbers of the composite system, respectively. The symbol α denotes the quantities of Z_1, N_1, Z_2, N_2, J, R, β_1, β_2, θ_1, θ_2. The $B(Z_i, N_i)(i = 1, 2)$ and $B(Z, N)$ are the negative binding energies of the fragment (Z_i, N_i) and the composite system (Z, N), respectively. The β_i represent the quadrupole deformations of the two fragments and are taken as the ground-state values. The θ_i denote the angles between the collision orientations and the symmetry axes of the deformed nuclei. Shown in Fig. 1 is the PES in the tip-tip collisions of ^{124}Sn + ^{238}U. The DNS fragments towards the mass symmetric valley release the positive energy, which are available for nucleon transfer. The spectra exhibit a symmetric distribution for each isotopic chain. The valley in the PES is close to the β-stability line and enables the diffusion of the fragment probability.

The total kinetic energy (TKE) of the primary fragment is evaluated by

$$\mathrm{TKE}(A_1) = E_{\mathrm{c.m.}} + Q_{gg}(A_1) - E^{\mathrm{diss}}(A_1), \tag{16}$$

where $Q_{gg} = M_P + M_T - M_{\mathrm{PLF}} - M_{\mathrm{TLF}}$ and $E_{\mathrm{c.m.}}$ is the incident energy in the center-of-mass frame. The mass M_P, M_T, M_{PLF}, and M_{TLF} correspond to projectile, target, projectilelike fragment, and targetlike fragment, respectively. The mass spectra of TKE is calculated as shown in Fig. 2 in the reaction of ^{124}Sn + ^{238}U. More broad TKE dissipation is pronounced in the range of PLFs and TLFs. The formation of DNS fragments tend to the symmetric pathway (quasifission process). The spectra exhibit a symmetric mass distribution because of the structure in the PES.

The emission angle of the reaction products is helpful for arranging detectors in experiments. We use a deflection function method to evaluate the fragment angle which is related to the mass of fragment, angular momentum, and incident energy. The deflection angle is composed of the Coulomb and nuclear interaction as [43,45]

$$\Theta(l_i) = \Theta(l_i)_C + \Theta(l_i)_N. \tag{17}$$

The Coulomb scattering angle is given by the Rutherford function. The nuclear deflection angle is evaluated by

$$\Theta(l_i)_N = \beta\Theta(l_i)_C^{gr}\frac{l_i}{l_{gr}}\left(\frac{\delta}{\beta}\right)^{l_i/l_{gr}}. \tag{18}$$

Here Θ_C^{gr} is the Coulomb scattering angle at the grazing angular momentum with $l_{gr} = 0.22R_{\mathrm{int}}[A_{\mathrm{red}}(E_{\mathrm{c.m.}} - V(R_{\mathrm{int}}))]^{1/2}$. The A_{red} and $V(R_{\mathrm{int}})$ correspond to the reduced mass of DNS fragments and interaction potential at the distance R_{int} of the entrance channel, respectively. The δ and β are parametrized

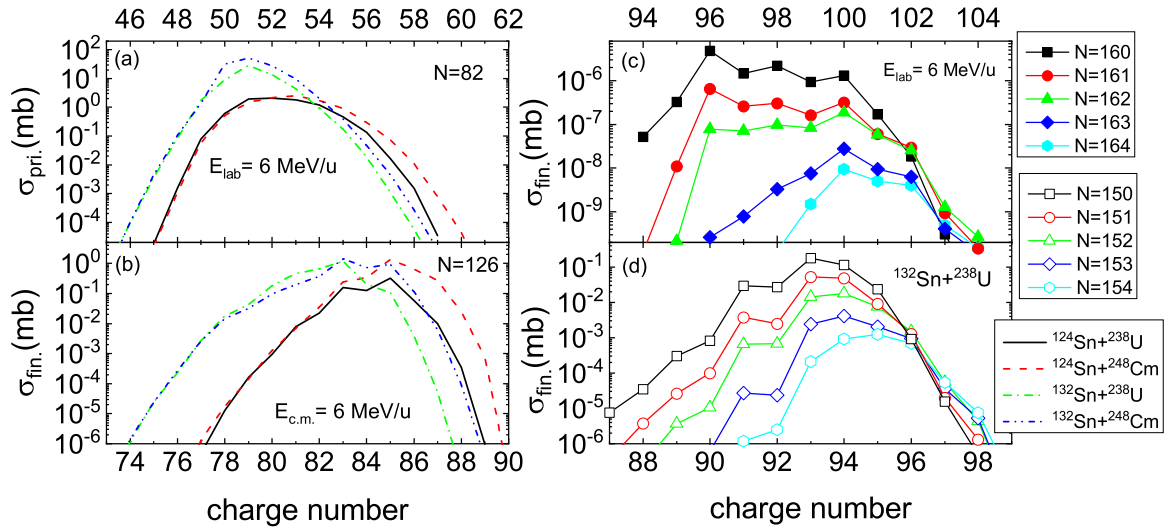

FIG. 8. Isotonic cross sections around neutron shell closure ($N = 82$ and 126) in the reactions of ^{124,132}Sn + ^{238}U/^{248}Cm (left panels) and the isotonic chains for the targetlike fragments in the reaction of ^{132}Sn + ^{238}U (right panels).

by fitting the deep inelastic scattering in massive collisions as

$$\beta = 75f(\eta) + 15, \quad \eta < 375,$$
$$36\exp(-2.17 \times 10^{-3}\eta), \quad \eta \geqslant 375, \tag{19}$$

$$\delta = 0.07f(\eta) + 0.11, \quad \eta < 375,$$
$$0.117\exp(-1.34 \times 10^{-4}\eta), \quad \eta \geqslant 375, \tag{20}$$

and

$$f(\eta) = \left[1 + \exp\frac{\eta - 235}{32}\right]^{-1}, \tag{21}$$

where $\eta = \frac{Z_1 Z_2 e^2}{\upsilon}$, and $\upsilon = \sqrt{\frac{2}{A_{\rm red}}(E_{\rm c.m.} - V(R_{\rm int}))}$.

III. RESULTS AND DISCUSSION

The damped collisions of two actinide nuclei were investigated and motivated for producing superheavy nuclei in the 1970s at Gesellschaft für Schwerionenforschung (GSI) [24,25]. Recently, the data were collected for investigating the MNT reactions, in particular for the transactinide production [46]. As a test of the DNS model, we calculated the isotopic cross sections in the reactions of ^{238}U + ^{238}U/^{248}Cm which are shown in Fig. 3. The isotopic yields are well reproduced with the model. It is obvious that the production cross section rapidly decreases with the actinide charge number. Up to 18 transferred nucleons were measured. The ^{248}Cm-based reactions are favorable for the transfermium isotope production owing to less nucleon transfer. To create SHN via MNT reactions, the heavy target nuclides are needed. The neutron shell closure is available for enhancing the transfer cross section in two actinide nuclide collisions. A bump structure of the isotopic yields around $N = 162$ was predicted [15], which is favorable for the neutron-rich SHN production.

The fragment yields in the MNT reactions are related to the emission angle in the laboratory system. It was observed that the clusters formed in massive transfer reactions are emitted anisotropically [47]. Accurate prediction of the polar angle structure for the MNT fragments is helpful for managing the detector system in experiments. Shown in Fig. 4 is the angular distribution of the primary MNT fragments produced in the reaction of ^{124}Sn + ^{238}U. The fragments are emitted in the forward region. The energy dependence of the projectilelike fragments (PLFs) in the mass region $A = 114$–134 and targetlike fragments (TLFs) with the mass number of $A = 228$–248 is opposite. The PLFs are emitted towards the forward angle region when increasing the incident energy. The emission angles of the maximal yields for PLFs and TLFs are close at the energy of 6.5 MeV/nucleon.

Neutron-rich Sn isotopes can be generated by the asymmetric fission of actinide nuclide, for instance, the new radioactive beam facility, Beijing Isotope Separation On Line (BISOL). The contour plot of primary and secondary fragments in collisions of ^{124,132}Sn + ^{238}U at the energy of 6 MeV/nucleon are calculated as shown in Fig. 5. The black zigzag line, straight line, and pentagram symbols correspond to the minimal values of each isotopic chain in the PES, linking line of entrance system, and position of projectile and target nuclides, respectively. The primary fragments are produced on the neutron-rich side. The de-excitation process moves the fragments to the β-stability line or even to the proton-rich domain. The nucleon transfer tends to the symmetric DNS fragments governed by the PES, in which the deformation, shell effect, and odd-even phenomena influence the dissipation process. The diffusion of primary fragments reaches the transfermium isotopes and even close to superheavy element Ds ($Z = 110$). Prompt de-excitation of primary fragments disenables the survival of SHN because of the low fission barriers. The PLFs and TLFs in the reaction ^{124}Sn + ^{238}U accumulate the neutron shell closure, i.e, around $N = 82$ and 152. The entrance system in the reaction ^{132}Sn + ^{238}U is positioned on the valley of the PES, which enables the nucleon diffusion along the zigzag line. The ^{132}Sn-induced reactions are favorable to produce neutron-rich

TABLE I. Cross sections of unknown neutron-rich heavy and superheavy isotopes with proton number Z and mass number A, predicted by the DNS model for the reactions of ^{124,132}Sn + ^{238}U/ ^{248}Cm around the Coulomb barrier energies from Nd to Rf. The last four columns show the number of new isotopes and their cross sections (in parentheses) which decrease with the increasing mass number.

Z (proton number)	A (mass number)	^{124}Sn+ ^{238}U(mb)	^{124}Sn+ ^{248}Cm(mb)	^{132}Sn+ ^{238}U(mb)	^{132}Sn+ ^{248}Cm(mb)
Nd(Z=60)	$A\geqslant$162	5 (10^{-5}–10^{-9})	5 (10^{-4}–10^{-9})	8 (10^{-2}–10^{-9})	8 (10^{-3}–10^{-9})
Pm(Z=61)	$A\geqslant$164	6 (10^{-4}–10^{-9})	6 (10^{-3}–10^{-9})	9 (10^{-1}–10^{-8})	10 (10^{-2}–10^{-9})
Sm(Z=62)	$A\geqslant$166	4 (10^{-5}–10^{-7})	4 (10^{-5}–10^{-8})	9 (10^{-2}–10^{-9})	9 (10^{-2}–10^{-9})
Eu(Z=63)	$A\geqslant$168	4 (10^{-5}–10^{-7})	4 (10^{-4}–10^{-8})	10 (10^{-2}–10^{-8})	10 (10^{-2}–10^{-8})
Gd(Z=64)	$A\geqslant$170	6 (10^{-5}–10^{-7})	5 (10^{-4}–10^{-8})	9 (10^{-2}–10^{-8})	9 (10^{-2}–10^{-8})
Tb(Z=65)	$A\geqslant$172	8 (10^{-4}–10^{-9})	6 (10^{-4}–10^{-9})	11 (10^{-1}–10^{-9})	10 (10^{-2}–10^{-9})
Dy(Z=66)	$A\geqslant$174	9 (10^{-3}–10^{-9})	8 (10^{-3}–10^{-9})	12 (10^{-1}–10^{-9})	11 (10^{-1}–10^{-9})
Ho(Z=67)	$A\geqslant$176	8 (10^{-3}–10^{-9})	7 (10^{-3}–10^{-9})	11 (10^{-1}–10^{-9})	10 (10^{-1}–10^{-9})
Er(Z=68)	$A\geqslant$178	7 (10^{-3}–10^{-8})	8 (10^{-4}–10^{-9})	11 (10^{-1}–10^{-9})	9 (10^{-2}–10^{-9})
Tm(Z=69)	$A\geqslant$181	7 (6×10^{-3}–10^{-9})	7 (10^{-3}–10^{-8})	12 (3×10^{-1}–10^{-9})	11 (10^{-1}–10^{-9})
Yb(Z=70)	$A\geqslant$185	4 (3×10^{-5}–10^{-8})	4 (10^{-5}–10^{-9})	10 (10^{-3}–10^{-9})	9 (10^{-3}–10^{-9})
Lu(Z=71)	$A\geqslant$188	3 (10^{-6}–10^{-9})	6 (10^{-6}–10^{-9})	8 (10^{-4}–10^{-9})	8 (10^{-4}–10^{-9})
Hf(Z=72)	$A\geqslant$190	1 (-10^{-8})	2 (10^{-8}–10^{-9})	7 (10^{-4}–10^{-9})	7 (10^{-4}–10^{-9})
Ta(Z=73)	$A\geqslant$194	1 (3.2×10^{-8})	2 (10^{-8}–10^{-9})	6 (10^{-4}–10^{-9})	7 (10^{-4}–10^{-9})
W(Z=74)	$A\geqslant$197	2 (10^{-7}–10^{-9})	3 (10^{-7}–10^{-9})	7 (10^{-3}–10^{-9})	7 (10^{-4}–10^{-9})
Re(Z=75)	$A\geqslant$199	2 (10^{-7}–10^{-9})	2 (10^{-7}–10^{-9})	7 (10^{-4}–10^{-9})	8 (10^{-4}–10^{-9})
Os(Z=76)	$A\geqslant$203	2 (10^{-7}–10^{-9})	2 (10^{-7}–10^{-9})	8 (10^{-4}–10^{-9})	8 (10^{-4}–10^{-9})
Ir(Z=77)	$A\geqslant$205	$<10^{-9}$	1 (10^{-8})	7 (10^{-4}–10^{-9})	7 (10^{-4}–10^{-9})
Pt(Z=78)	$A\geqslant$208	2 (10^{-7}–10^{-9})	3 (10^{-7}–10^{-9})	9 (10^{-3}–10^{-9})	9 (10^{-3}–10^{-9})
Au(Z=79)	$A\geqslant$211	$<10^{-9}$	1 (-10^{-9})	7 (10^{-4}–10^{-9})	7 (10^{-4}–10^{-8})
Hg(Z=80)	$A\geqslant$217	5 (10^{-5}–10^{-9})	5 (10^{-4}–10^{-9})	8 (10^{-2}–10^{-9})	8 (10^{-3}–10^{-9})
Tl(Z=81)	$A\geqslant$218	$<10^{-9}$	$<10^{-9}$	4 (10^{-6}–10^{-9})	4 (10^{-6}–10^{-9})
Pb(Z=82)	$A\geqslant$221	$<10^{-9}$	$<10^{-9}$	3 (10^{-5}–10^{-9})	4 (10^{-5}–10^{-9})
Bi(Z=83)	$A\geqslant$225	$<10^{-9}$	$<10^{-9}$	3 (10^{-5}–10^{-7})	4 (10^{-5}–10^{-9})
Po(Z=84)	$A\geqslant$227	$<10^{-9}$	$<10^{-9}$	3 (10^{-6}–10^{-9})	3 (10^{-6}–10^{-9})
At(Z=85)	$A\geqslant$230	$<10^{-9}$	$<10^{-9}$	7 (10^{-4}–10^{-9})	5 (10^{-5}–10^{-9})
Rn(Z=86)	$A\geqslant$232	$<10^{-9}$	$<10^{-9}$	5 (10^{-5}–10^{-9})	3 (10^{-6}–10^{-9})
Fr(Z=87)	$A\geqslant$234	2 (10^{-7}–10^{-9})	2 (-10^{-8})	5 (10^{-4}–10^{-7})	4 (10^{-6}–10^{-9})
Ra(Z=88)	$A\geqslant$235	4 (10^{-5}–10^{-9})	3 (10^{-6}–10^{-9})	7 (10^{-2}–10^{-9})	5 (10^{-4}–10^{-9})
Ac(Z=89)	$A\geqslant$238	5 (10^{-4}–10^{-9})	6 (10^{-3}–10^{-9})	9 (1.6–10^{-9})	9 (10^{-2}–10^{-9})
Th(Z=90)	$A\geqslant$240	2 (10^{-5}, 10^{-7})	4 (10^{-4}–10^{-7})	6 (10^{-3}–10^{-9})	7 (10^{-3}–10^{-9})
Pa(Z=91)	$A\geqslant$242	3 (10^{-5}–10^{-7})	5 (10^{-3}–10^{-7})	7 (10^{-1}–10^{-8})	9 (10^{-1}–10^{-8})
U(Z=92)	$A\geqslant$244	4 (10^{-5}–10^{-9})	7 (10^{-2}–10^{-8})	8 (10^{-1}–10^{-9})	11 (10^{-1}–10^{-9})
Np(Z=93)	$A\geqslant$245	3 (10^{-6}–10^{-9})	3 (10^{-4}–10^{-9})	7 (10^{-2}–10^{-9})	8 (1–10^{-9})
Pu(Z=94)	$A\geqslant$248	3 (10^{-6}–10^{-9})	2 (10^{-6}–10^{-8})	7 (10^{-3}–10^{-8})	7 (10^{-3}–10^{-9})
Am(Z=95)	$A\geqslant$250	5 (10^{-5}–10^{-9})	4 (10^{-3}–10^{-7})	9 (10^{-3}–10^{-8})	9 (26–10^{-8})
Cm(Z=96)	$A\geqslant$253	3 (10^{-6}–10^{-9})	2 (10^{-7}–10^{-9})	7 (10^{-4}–10^{-8})	6 (10^{-3}–10^{-8})
Bk(Z=97)	$A\geqslant$255	2 (10^{-7}–10^{-9})	3 (10^{-6}–10^{-9})	6 (10^{-5}–10^{-7})	7 (10^{-4}–10^{-8})
Cf(Z=98)	$A\geqslant$257	1 (1.8×10^{-9})	3 (10^{-7}–10^{-9})	5 (10^{-6}–10^{-9})	6 (10^{-5}–10^{-9})
Es(Z=99)	$A\geqslant$259	$<10^{-9}$	4(10^{-7}–10^{-9})	6 (10^{-7}–10^{-9})	6 (10^{-6}–10^{-9})
Fm(Z=100)	$A\geqslant$261	$<10^{-9}$	2(10^{-8}–10^{-9})	4 (10^{-7}–10^{-9})	6 (10^{-7}–10^{-9})
Md(Z=101)	$A\geqslant$261	1 (1.3×10^{-9})	3 (10^{-7}–10^{-9})	5 (10^{-7}–10^{-9})	5 (10^{-8}–10^{-9})
No(Z=102)	$A\geqslant$265	1 (2×10^{-9}))	4 (10^{-7}–10^{-9})	6 (10^{-8}–10^{-9})	8 (10^{-8}–10^{-9})
Lr(Z=103)	$A\geqslant$267	2 (1×10^{-9})	5 (10^{-8}–10^{-9})	1 (1×10^{-9})	1 (1×10^{-9})
Rf(Z=104)	$A\geqslant$269	$<10^{-9}$	2(1×10^{-9})	0 ($<10^{-9}$)	5 (1×10^{-9})

nuclei. Accurate estimations of the fission barrier for actinide and transfermium nuclides are of importance for calculating the production cross section in the MNT reactions. The multidimensionally constrained covariant density functional approach was attempted to estimate the fission barrier of the actinide nucleus [48].

The production cross sections of MNT fragments are related to the reaction systems, in which the shell effect and isospin relaxation play significant roles on the fragment formation [49,50]. The fragments in the pre-equilibrium process are produced around the projectile- or targetlike regions. More dissipations are available for creating the SHN and medium fragments. The nucleon transfer tends to the pathway along the valley in PES. Shown in Fig. 6 are the isotopic spectra of production cross sections in the MNT reactions with ^{124}Sn and ^{132}Sn on ^{238}U at the energy of 6 MeV/nucleon. The maximal yields move to the neutron-rich side for the proton pickup (left panels) and stripping (right

panels) reactions with the bombarding nuclide ^{132}Sn. The proton stripping reactions need to overcome the inner barrier in the PES and thus the cross sections drop rapidly with the proton number, e.g., μb for four protons stripping from the bombarding nuclide. More nucleon transferring is needed for creating the transfermium isotopes.

Figure 7 shows the cross sections for isotopes $Z = 101$–104 in the MNT reactions of ^{124,132}Sn + ^{238}U/^{248}Cm. In the left panels it is shown that the cross sections induced by ^{124}Sn have similar shapes and magnitudes with that induced by ^{132}Sn, but the peak values shift towards the neutron-rich side for the latter case. However, for the spectra of ^{248}Cm-based reactions, the situation is somewhat complicated. The magnitudes are quite different for isotopes $Z = 101$–103 with different projectiles. The peak values in ^{132}Sn-induced reactions are typically 1–2 order smaller than that induced by ^{124}Sn. This is caused by the fact that a shape transition from prolate to oblate ellipsoid takes place around $A = 110$ for projectilelike isotopes Rh, Ru, and Tc, which increase the interaction potential and enlarge the inner transfer barrier, and finally reduce the cross section significantly. The MNT reaction of ^{132}Sn + ^{248}Cm is a promising pathway for producing the neutron-rich transfermium nuclides, in particular around the region of $N = 162$. The nuclear spectroscopy and decay modes of the transfermium isotopes are the stepstone for investigating the SHN properties.

The isotonic cross sections in the four systems ^{124,132}Sn + ^{238}U/^{248}Cm at incident energy of 6 MeV/nucleon are calculated as shown in Fig. 8. It is obvious that the structure of the MNT yields is dependent on the projectile-target combinations. On the proton-rich side, the production cross section is enhanced with enlarging the mass asymmetry of the entrance system. The neutron-rich isotopes around $N = 82$ and 126 are solely associated with the bombarding nuclide. The cross sections of the neutron-rich nuclide are enhanced in the ^{132}Sn-induced reactions. The reaction systems reach the isospin equilibrium in the final evolution. The neutron to proton ratios are 1.548, 1.549, 1.603, and 1.605 for the reactions ^{124}Sn + ^{248}Cm, ^{124}Sn + ^{238}U, ^{132}Sn + ^{248}Cm, and ^{132}Sn + ^{238}Cm, respectively. The isotonic distribution around the subshell closures $N = 152$ and 162 is shown in the right panels for the reaction ^{132}Sn + ^{238}U. The difference of isotonic cross sections is pronounced in the neutron-rich domain. It is caused by the fact that the large N/Z ratios of isotopes in the neutron-rich region are away from the average value of the reaction system. However, the isospin ratios of heavy isotopes are close to the N/Z value of the colliding system.

New isotopes might be produced via the MNT reactions. The cross sections are estimated as shown in Table I for four systems of ^{124}Sn + ^{238}U, ^{124}Sn + ^{248}Cm, ^{132}Sn + ^{238}U, and ^{132}Sn + ^{248}Cm at incident energy $E_{lab} = 6$ MeV/u. The production cross section at the level of pb is feasible for measurements in laboratories. The number of new isotopes is indicated for the reaction systems. The new isotopic chains are broad with the ^{132}Sn-induced reactions. Further measurements are expected in the future experiments.

IV. CONCLUSIONS

In summary, the production of neutron-rich isotopes via the MNT reactions was investigated within the DNS model for the reaction systems of ^{124,132}Sn + ^{238}U/^{248}Cm around Coulomb barrier energies. The nucleon transfer takes place at the touching configuration of two fragments under the PES. The valley shape of the PES influences the formation of primary fragments and leads to the production of neutron-rich isotopes. The de-excitation process shifts the neutron excess of fragments towards the β-stability line. The isospin relaxation in the nucleon transfer is coupled to the dissipation of relative energy and angular momentum of the colliding system. The available experimental data for two actinide nuclide collisions are well reproduced. The fragment yields are enhanced around the shell closure. The neutron-rich nucleus ^{132}Sn ($n/p = 1.62$) induced reactions are favorable to produce heavy neutron-rich isotopes around TLFs. The anisotropy emission of MNT fragments is associated with the incident energy of the colliding system. The angular distribution of the PLFs is shifted to the forward region with increasing the beam energy. However, that of TLFs exhibits an opposite trend. The production cross sections of isotonic chains around the neutron shell closure $N = 82$ and 126 depend on the projectile-target combinations, in particular in the proton-rich domain. The difference between the isotonic cross sections around $N = 152$ and 162 is pronounced in the neutron-rich region. The isotopic cross sections of Nd, Gd, and Pb are related to the entrance channel effect. Predicted numerous unknown neutron-rich nuclei from $Z = 60$ to $Z = 104$ predicted with the cross section by the DNS model within four reaction systems, which are list in Table I. The ^{132}Sn-induced reactions are available for the neutron-rich isotope production. Possible measurements are expected in future experiments.

ACKNOWLEDGMENTS

This work was supported by the National Natural Science Foundation of China (Grants No. 11675226, No. 11722546, and No. 11975282) and the Talent Program of South China University of Technology.

[1] G. Münzenberg and K. Morita, Synthesis of the heaviest nuclei in cold fusion reactions, Nucl. Phys. A **944**, 3 (2015); G. Münzenberg, From bohrium to copernicium and beyond SHE research at SHIP, *ibid.* **944**, 5 (2015).

[2] Yu. Ts. Oganessian and V. K. Utyonkov, Superheavy nuclei from 48Ca-induced reactions, Nucl. Phys. A **944**, 62 (2015).

[3] S. Heinz, Multinucleon transfer reactions - a pathway to new heavy and superheavy nuclei? J. Phys. G: Conf. Ser. **1014**, 012005 (2005).

[4] V. Zagrebaev and W. Greiner, Low-energy collisions of heavy nuclei: dynamics of sticking, mass transfer and fusion, J. Phys. G **34**, 1 (2007); New way for the production of heavy neutron-rich nuclei, **35**, 125103 (2008).

[5] J. S. Barrett, W. Loveland, R. Yanez, S. Zhu, A. D. Ayangeakaa, M. P. Carpenter, J. P. Greene, R. V. F. Janssens, T. Lauritsen, E. A. McCutchan, A. A. Sonzogni, C. J. Chiara, J. L. Harker, and W. B. Walters, ^{136}Xe+^{208}Pb reaction: A test of models of multinucleon transfer reactions, Phys. Rev. C **91**, 064615 (2015).

[6] Y. X. Watanabe *et al.*, Pathway for the Production of Neutron-Rich Isotopes around the N = 126 Shell Closure, Phys. Rev. Lett. **115**, 172503 (2015).

[7] V. Zagrebaev and W. Greiner, Synthesis of superheavy nuclei: A search for new production reactions, Phys. Rev. C **78**, 034610 (2008); Production of New Heavy Isotopes in Low-Energy Multinucleon Transfer Reactions, Phys. Rev. Lett. **101**, 122701 (2008).

[8] C. Golabek and C. Simenel, Collision Dynamics of Two ^{238}U Atomic Nuclei, Phys. Rev. Lett. **103**, 042701 (2009).

[9] K. Sekizawa and K. Yabana, Time-dependent Hartree-Fock calculations for multinucleon transfer and quasifission processes in the ^{64}Ni+^{238}U reaction, Phys. Rev. C **93**, 054616 (2016).

[10] L. Guo, C. Simenel, L. Shi, and C. Yu, The role of tensor force in heavy-ion fusion dynamics, Phys. Lett. B **782**, 401 (2018).

[11] X. Jiang and N. Wang, Production mechanism of neutron-rich nuclei around N = 126 in the multi-nucleon transfer reaction ^{132}Sn + ^{208}Pb, Chin. Phys. C **42**, 104105 (2018).

[12] A. Winther, Grazing reactions in collisions between heavy nuclei, Nucl. Phys. A **572**, 191 (1994); Dissipation, polarization and fluctuation in grazing heavy-ion collisions and the boundary to the chaotic regime, **594**, 203 (1995).

[13] http://www.to.infn.it/nanni/grazing

[14] K. Zhao, Z. Li, N. Wang, Y. Zhang, Q. Li, Y. Wang, and X. Wu, Production mechansim of neutron-rich transuranium nuclei in ^{238}U+^{238}U, Phys. Rev. C **92**, 024613 (2015).

[15] Z. Q. Feng, G. M. Jin, and J. Q. Li, Production of heavy isotopes in transfer reactions by collisions of ^{238}U+^{238}U, Phys. Rev. C **80**, 067601 (2009).

[16] G. G. Adamian, N. V. Antonenko, V. V. Sargsyan, and W. Scheid, Possibility of production of neutron-rich Zn and Ge isotopes in multinucleon transfer reactions at low energies, Phys. Rev. C **81**, 024604 (2010); Predicted yields of new neutron-rich isotopes of nuclei with $Z = 64$–80 in the multinucleon transfer reaction ^{48}Ca+^{238}U, **81**, 057602 (2010).

[17] C. H. Dasso, G. Pollaro, and A. Winther, Systematics of Isotope Production with Radioactive Beams, Phys. Rev. Lett. **73**, 1907 (1994); Particle evaporation following multinucleon transfer process with radioactive beams, Phys. Rev. C **52**, 2264 (1995).

[18] V. Zagrebaev and W. Greiner, Cross sections for the production of superheavy nuclei, Nucl. Phys. A **944**, 257 (2015).

[19] M.-H. Mun, G. G. Adamian, N. V. Antonenko, Y. Oh, and Y. Kim, Toward neutron-rich nuclei via transfer reactions with stable and radioactive beams, Phys. Rev. C **91**, 054610 (2015).

[20] L. W. David, The synthesis of new neutron-rich heavy nuclei, Front. Phys. **7**, 23 (2019).

[21] A. G. Artukh, V. V. Avdeichikov, G. F. Gridnev, V. L. Mikheev, V. V. Volkov, and J. Wilczynski, New isotopes ^{29,30}Mg, ^{31,32,33}Al, ^{33,34,35,36}Si, ^{35,36,37,38}P, ^{39,40}S and ^{41,42}Cl produced in bombardment of a ^{232}Th target with 290 MeV ^{40}Ar ions, Nucl. Phys. A **176**, 284 (1971).

[22] A. G. Artukh, G. F. Gridnev, V. L. Mikheev, V. V. Volkov, and J. Wilczynski, Multinucleon transfer reactions in the ^{232}Th+^{22}Ne system, Nucl. Phys. A **211**, 299 (1973).

[23] A. G. Artukh, G. F. Gridnev, V. L. Mikheev, V. V. Volkov, and J. Wilczynski, Transfer reactions in the interaction of ^{40}Ar with ^{232}Th, Nucl. Phys. A **215**, 91 (1973).

[24] K. D. Hildenbrand, H. Freiesleben, F. Phlhofer, W. F. W. Schneider, R. Bock, D. V. Harrach, and H. J. Specht, Reaction between ^{238}U and ^{238}U at 7.42 MeV Nucleon, Phys. Rev. Lett. **39**, 1065 (1977).

[25] P. Glässel, D. V. Harrach, Y. Civelekoglu, R. Männer, H. J. Specht, J. B. Wilhelmy, H. Freiesleben, and K. D. Hildenbrand, Three-Particle Exclusive Measurements of the Reactions ^{238}U+^{238}U and ^{238}U+^{248}Cm, Phys. Rev. Lett. **43**, 1483 (1979).

[26] K. J. Moody, D. Lee, R. B. Welch, K. E. Gregorich, G. T. Seaborg, R. W. Lougheed, and E. K. Hulet, Actinide production in reactions of heavy ions with ^{248}Cm, Phys. Rev. C **33**, 1315 (1986).

[27] R. B. Welch, K. J. Moody, K. E. Gregorich, D. Lee, and G. T. Seaborg, Dependence of actinide production on the mass number of the projectile: Xe+^{248}Cm, Phys. Rev. C **35**, 204 (1987).

[28] E. M. Kozulin, E. Vardaci, G. N. Knyazheva, A. A. Bogachev, S. N. Dmitriev, I. M. Itkis, M. G. Itkis, A. G. Knyazev, T. A. Loktev, K. V. Novikov, E. A. Razinkov, O. V. Rudakov, S. V. Smirnov, W. Trzaska, and V. I. Zagrebaev, Mass distributions of the system ^{136}Xe+^{208}Pb at laboratory energies around the Coulomb barrier: A candidate reaction for the production of neutron-rich nuclei at $N = 126$, Phys. Rev. C **86**, 044611 (2012).

[29] E. M. Kozulin, V. I. Zagrebaev, G. N. Knyazheva, I. M. Itkis, K. V. Novikov, M. G. Itkis, S. N. Dmitriev, I. M. Harca, A. E. Bondarchenko, A. V. Karpov, M. G. Itkis, S. N. Dmitriev, I. M. Harca, A. E. Bondarchenko, A. V. Karpov, V. V. Saiko, and E. Vardaci, Inverse quasifission in the reactions ^{156,160}Gd+^{186}W, Phys. Rev. C **96**, 064621 (2017).

[30] S. Wuenschel, K. Hagel, M. Barbui, J. Gauthier, X. G. Cao, R. Wada, E. J. Kim, Z. Majka, R. Planeta, Z. Sosin, A. Wieloch, K. Zelga, S. Kowalski, K. Schmidt, C. Ma, G. Zhang, and J. B. Natowitz, Experimental survey of the production of α-decaying heavy elements in ^{238}U+^{232}Th reactions at 7.5–6.1 MeV/nucleon, Phys. Rev. C **97**, 064602 (2018).

[31] J. C. Yang, J. W. Xia, G. Q. Xiao *et al.*, High Intensity heavy ion Accelerator Facility (HIAF) in China, Nucl. Instrum. Methods B **317**, 263 (2013).

[32] V. V. Volkov, Deep inelastic transfer reactions- The new type of reactions between complex nuclei, Phys. Rep. **44**, 93 (1978).

[33] G. G. Adamian, N. V. Antonenko, W. Scheid *et al.*, Treatment of competition between complete fusion and quasifission in collisions of heavy nuclei, Nucl. Phys. A **627**, 361 (1997).

[34] G. G. Adamian, N. V. Antonenko, W. Scheid *et al.*, Fusion cross sections for superheavy nuclei in the dinuclear system concept, Nucl. Phys. A **633**, 409 (1998).

[35] W. Li, N. Wang, J. F. Li *et al.*, Fusion probability in heavy-ion collisions by a dinuclear-system model, Europhys. Lett. **64**, 750 (2003).

[36] Z. Q. Feng, G. M. Jin, F. Fu *et al.*, Entrance channel dependence of production cross sections of superheavy nuclei in cold fusion reactions, Chin. Phys. Lett. **22**, 846 (2005).

[37] Z. Q. Feng, G. M. Jin, F. Fu, and J. Q. Li, Production cross sections of superheavy nuclei based on dinuclear system model, Nucl. Phys. A **771**, 50 (2006); Z. Q. Feng, G. M. Jin, J. Q. Li, and W. Scheid, Formation of superheavy nuclei in cold fusion reactions, Phys. Rev. C **76**, 044606 (2007).

[38] Z. Q. Feng, G. M. Jin, and J. Q. Li, Production of new superheavy Z = 108–114 nuclei with ^{238}U, ^{244}Pu, and ^{248,250}Cm targets, Phys. Rev. C **80**, 057601 (2009); Z. Q. Feng, G. M. Jin, J. Q. Li, and W. Scheid, Production of heavy and superheavy nuclei in massive fusion reactions, Nucl. Phys. A **816**, 33 (2009).

[39] Z. Q. Feng, G. M. Jin, and J. Q. Li, Influence of entrance channels on the formation of superheavy nuclei in massive fusion reactions, Nucl. Phys. A **836**, 82 (2010).

[40] P. H. Chen, Z. Q. Feng, J. Q. Li, and H. F. Zhang, A statistical approach to describe highly excited heavy and superheavy nuclei, Chin. Phys. C **40**, 091002 (2016).

[41] V. Yu. Denisov and W. Nörenberg, Entrance channel potentials in the synthesis of the heaviest nuclei, Eur. Phys. J. A **15**, 375 (2002).

[42] W. Nörenberg, Quantum-statistical approach to gross properties of peripheral collisions between heavy nuclei, Z. Phys. A **274**, 241 (1975); S. Ayik, B. Schürmann, and W. Nörenberg, Microscopic transport theory of heavy-ion collisions, *ibid.* **277**, 299 (1976).

[43] G. Wolschin and W. Nörenberg, Analysis of relaxation phenomena in heavy-ion collisions, Z. Phys. A **284**, 209 (1978).

[44] Z. Q. Feng, G. M. Jin, F. Fu, and J. Q. Li, Isotopic dependence of production cross sections of superheavy nuclei in hot fusion reactions, Chin. Phys. C **31**, 366 (2007).

[45] P. H. Chen, F. Niu, Y. F. Guo, and Z. Q. Feng, Nuclear dynamics in multinucleon transfer reactions near Coulomb barrier energies, Nucl. Sci. Tech. **29**, 185 (2018).

[46] J. V. Kratz, M. Schädel, and H. W. Gäggeler, Reexamining the heavy-ion reactions ^{238}U+^{238}U and ^{238}U+^{248}Cm and actinide production close to the barrier, Phys. Rev. C **88**, 054615 (2013).

[47] G. M. Jin, Y. X. Xie, Y. T. Zhu *et al.*, Product cross sections for the reaction of ^{12}C with ^{209}Bi, Nucl. Phys. A **349**, 285 (1980).

[48] S. G. Zhou, Multidimensionally constrained covariant density functional theories—nuclear shapes and potential energy surfaces, Phys. Scr. **91**, 063008 (2016).

[49] Z.-Q. Feng, Production of neutron-rich isotopes around N = 126 in multinucleon transfer reactions, Phys. Rev. C **95**, 024615 (2017).

[50] F. Niu, P.-H. Chen, Y.-F. Guo, C.-W. Ma, and Z.-Q. Feng, Multinucleon transfer dynamics in heavy-ion collisions near Coulomb-barrier energies, Phys. Rev. C **96**, 064622 (2017); Effect of isospin diffusion on the production of neutron-rich nuclei in multinucleon transfer reactions, **97**, 034609 (2018).